SEMARAK ILMU PUBLISHING

CFD Letters

Journal homepage:
https://semarakilmu.com.my/journals/index.php/CFD_Letters/index
ISSN: 2180-1363

Numerical Investigation of Underwater Vehicle Maneuvering under Static Drift Conditions

Muhammad Sajjad Ahmad[1], Muhammed Amirul Asyraf Hasnan[1,*], Nik Mohd Ridzuan Shaharuddin[1], Muhammad Noor Afiq Witri Muhammad Yazid[1], Imran Shah[2], Nauman Bashir[3]

[1] Faculty of Mechanical Engineering, Universiti Teknologi Malaysia, 81310, Skudai, Johor, Malaysia
[2] Department of Mechatronics Engineering, Air University, Islamabad, 44000, Pakistan
[3] Department of Industrial & Manufacturing Engineering, PNEC, National university of Sciences and Technology, Karachi,07548, Pakistan

ARTICLE INFO

Article history:
Received 19 August 2024
Received in revised form 19 September 2024
Accepted 20 October 2024
Available online 30 November 2024

Keywords:
Underwater vehicle; static drift; hydrodynamic behavior; maneuverability; DARPA suboff

ABSTRACT

The hydrodynamic behavior of underwater vehicles is crucial for achieving optimal maneuverability and energy efficiency in various underwater environments, thereby ensuring effective underwater operations. This research addresses the drift characteristics of an underwater vehicle by conducting Computational Fluid Dynamics (CFD) simulations. DARPA Suboff model was used to analyze its maneuvering characteristics under static drift conditions at a velocity of 3.34 m/s and drift angles ranging from 0 to 18 degrees with 2-degree intervals. The simulations replicate actual sea conditions using the Reynolds-Averaged Navier-Stokes (RANS) equations combined with the k-ω Shear Stress Transport (SST) turbulence model. The computational domain and boundary conditions are carefully defined to optimize the computational cost. The results revealed a significant decrease in longitudinal force when the drift angle increased, while the lateral force and yaw moment showed substantial increases, indicating the complex interactions between drift angles and hydrodynamic performance. This research provides valuable insights into the hydrodynamic forces and moments acting on underwater vehicles, contributing to their design optimization for improved stability and efficiency.

1. Introduction

Underwater vehicles are widely being used for military, research, equipment installation, or maintenance purposes. It requires a comprehensive evaluation of maneuvering characteristics for operational success and safety of autonomous underwater vehicles. Various methods have been developed to estimate these characteristics with high precision. Empirical and semi-empirical approaches are frequently used during the preliminary design phases to ascertain hydrodynamic characteristics, due to their economical nature and adaptability for necessary modifications [1]. They provide a practical starting point for understanding the basic maneuvering capabilities of underwater vehicles without incurring significant expenses. While experimental techniques tend to incur higher

* *Corresponding author.*
E-mail address: muhammedamirulasyraf@utm.my (Muhammed Amirul Asyraf Hasnan)

https://doi.org/10.37934/cfdl.17.5.4557

costs and demand considerable time, they yield the most dependable results by integrating the non-linear dynamics prevalent in real-world scenarios, thereby rendering them particularly suitable for the validation of other methods [2]. Numerical techniques, especially Computational Fluid Dynamics (CFD), have emerged as a prominent tool due to their capacity to swiftly and economically simulate forces, velocities, pressures, and turbulence in situations where the acquisition of experimental data proves to be challenging[3-6]. CFD simulations have been effectively used to study the maneuvering of underwater vehicles, optimizing computational costs to facilitate application in the concept design phase [7, 8]. Additionally, CFD has been employed to adapt Karasuno's fishery vessel maneuvering model to underwater vehicles, providing accurate representations of forces and moments during large drift and angle of attack motions [9].

Groves *et al.,* [10] suggested to the DARPA Suboff geometry as a recommended hull form for conducting benchmark tests on underwater vehicles. Roddy [11] conducted towing tank experiments on different configurations of DARPA Suboff to investigate stability and control characteristics. Huang and Liu [12] performed wind tunnel tests on Suboff model and presented flow measurements over hull with various appendages. Different configurations of DARPA Suboff model are widely used in underwater vehicles research studies. The DARPA Suboff model is predominantly favored in benchmark underwater vehicles due to its streamlined and hydrodynamic hull design. Its utility is noteworthy due to the extensive research available in the published literature. The ITTC-Maneuvering Committee(2014), also recommends researchers to use the DARPA Suboff geometry [13].

Toxopeus and Vaz [14] analyzed the flow at various drift angles around the bare hull of the DARPA Suboff. They employed their own code and implemented different turbulence models. Vaz *et al.,* [15] conducted a study using CFD to ascertain the maneuvering forces of the DARPA SUBOFF. They applied two viscous-flow solvers Reynolds-Averaged-Navier-Stokes (RANS) and more advanced Delayed-Detached-Eddy-Simulation (DDES) to ensure precise predictions of forces and moments for the AFF-1(barehull) and AFF-8(fully appended) configurations at 0° and 18° angles for static drift. They also examined the effects of appendages on the resulting forces and flow fields. This foundational work laid the groundwork for further exploration into the hydrodynamic behavior of underwater vehicles, emphasizing the importance of turbulence modeling in predicting flow characteristics accurately.

Pan *et al.,* [16] conducted both steady and unsteady RANS simulations alongside the oblique towing tank and planar motion mechanism (PMM) experiments on the SUBOFF model. Their findings indicated a strong agreement of CFD results with experimental data. Although it was noted that the PMM experiment is the most effective method, it is also resource-intensive and may not be feasible during the initial design phase. Atik [17] determined that while turbulence models yielded similar results at small angles, the discrepancies increased with angle. Tat *et al.,* [18] investigated four turbulence models for resistance of DARPA-Suboff and found that k-ω SST turbulence model provide more accurate results. Firdhaus *et al.,* [19] found k-w SST turbulence model, most suitable to simulate the flow around a hydrofoil-supported hull form. The k-ω SST (Shear Stress Transport) model provides the most accurate findings, revealing a 10% average difference between numerical and experimental outcomes beyond 8 degrees of static drift.

Despite the popularity of experimental methods to estimate hydrodynamic coefficients, their excessive costs, mainly due to extensive number of 6-DoF captive matrix measurements required, make this approach impractical for small-sized vehicles operating on a limited budget. Meanwhile, that expense barrier makes it extremely unlikely to run such experiments in preliminary design stages. Furthermore, the effect of the support structure is very critical during experiments. The presence of struts can greatly affect the flow around an underwater vehicle model, even though only hydrodynamic forces are measured on the model itself. Other complications go beyond support

struts, such as boundary effects from tank walls and the bottom, which can alter measurement repeatability. Finally, wave interference within the towing tank introduces additional complexity in isolating intended hydrodynamic responses. However, CFD methods provides the advantage of estimating hydrodynamics of an underwater vehicle with presence of support struts. CFD allows for calculation of forces on individual appendages of underwater vehicles, such as rudders, sail, fins etc. without the complication of measuring devices used for experiments [20,21]. However, CFD techniques also have disadvantages, including significant computational expenses when handling complex geometries and the need to keep pace with the continual and rapid advancements in numerical techniques and simulation frameworks.

Although extensive study has been conducted on the various configurations of DARPA Suboff model, it is essential to accurately estimate the hydrodynamic forces and moments acting on fully appended geometry, e.g. AFF-8 during static drift situations. The focus of this study is to perform maneuvering analysis of the AFF-8 configurations using CFD simulations. The analysis is conducted for drift angles varying from 0° to 18°, with a speed of 3.343 m/s. The forces and moments involved in maneuvering are calculated for various drift angles, and the accuracy of the CFD methods is confirmed by comparing the results with the experimental results. The results are converted to non-dimensional values in order to allow comparison with the experimental data of DTRC [11]. Since the DARPA Suboff is symmetrical along the y-axis, calculations are conducted exclusively for one side. Consequently, the primary aim of this research is to study the forces and moments on AFF-8 (fully appended DARPA Suboff) geometry in the static drift condition, and determination of maneuvering derivatives from the obtained forces and moment values.

2. Methodology

The 6DOF maneuvering motion is decoupled into three horizontal and three vertical components. This is done to simplify the prediction of hydrodynamic forces and moments acting on underwater vehicles. This simplification allows the complex dynamics to be represented as a set of linear equations, facilitating easier analysis and computation [22]. The accurate estimation of hydrodynamic coefficients is crucial, as these coefficients characterize the forces and moments specific to the vehicle's shape and motion. Moreover, understanding the 6DOF motion in three-dimensional space is vital for capturing the full range of vehicle dynamics.

2.1 Maneuvering Equations

The generalized 6-DoF rigid-body equations of motion in a body-fixed, non-inertial frame of reference X Y Z that is in motion relative to an Earth-fixed, inertial reference frame $X_0\ Y_0\ Z_0$ can be derived as follows [23]:

$$m[\dot{u} - vr + \omega q - x_G(q^2 + r^2) + y_G(pq - \dot{r}) + z_G(pr + \dot{q})] = X \tag{1}$$

$$m[\dot{v} - \omega p + ur - y_G(r^2 + p^2) + z_G(qr - \dot{p}) + x_G(qp + \dot{r})] = Y \tag{2}$$

$$m[\dot{\omega} - uq + vp - z_G(p^2 + q^2) + x_G(rp - \dot{q}) + y_G(rq + \dot{p})] = Z \tag{3}$$

$$I_x\dot{p} + (I_z - I_y)qr - (r + pq)I_{xz} + (r^2 - q^2)I_{yz} + (pr - \dot{q})I_{xy} + m[y_G(\dot{\omega} - uq + vp) - z_G(\dot{v} - \omega p + ur)] = K \tag{4}$$

$$I_y\dot{q} + (I_x - I_z)rp - (\dot{p} + qr)I_{xy} + (p^2 - r^2)I_{zx} + (qp - \dot{r})I_{yz} + m[z_G(\dot{u} - vr + \omega q) - x_G(\dot{\omega} - uq + vp)] = M \quad (5)$$

$$I_z\dot{r} + (I_y - I_x)pq - (\dot{q} + rp)I_{yz} + (q^2 - p^2)I_{xy} + (rq - \dot{p})I_{zx} + m[x_G(\dot{v} - \omega p + ur) - y_G(\dot{u} - vr + \omega q)] = N \quad (6)$$

Eq. (1), Eq. (2), and Eq. (3) explain the translational motions of surge-x, sway-y, and heave-z and whereas Eq. (4), Eq. (5), and Eq. (6) respectively describe the rotating motions of roll-ϕ, pitch-ϑ and yaw-ψ. These 6-DoF equations of motion describe the external forces (X, Y, Z) and external moments (K, M, N) acting on the underwater vehicle. Maneuvering studies incorporate two coordinate systems; an inertial coordinate system (x_0, y_0, z_0) fixed on earth and a moving coordinate system (x, y, z) fixed on body. Similarly, m is mass of the vehicle and $I_X\ I_Y\ I_Z$ are the vehicle's moments of inertia. Centre of gravity (CoG) of underwater vehicle is defined by the points (x_G, y_G, z_G). The current study employs a coordinate system where the x-axis represents the longitudinal axis of the vehicle, with the bow pointing in the positive x direction. The y-axis represents the port (PS) and starboard (SB) sides of the underwater vehicle. The z-axis is oriented vertically relative to the vehicle, with the positive direction pointing downward. Description of the coordinates is shown in Figure 1. which is utilized in moment estimates along the z-axis, is estimated based on the center of gravity (COG) of the model at 0.4621*L_{OA} from the bow of the vehicle.

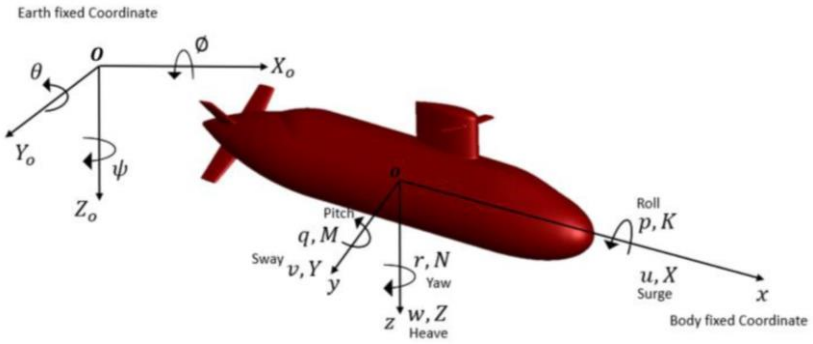

Fig. 1. Coordinated of Underwater vehicle [24]

When forces and moments acting on the body are considered in the horizontal plane for any underwater vehicle, the roll, heave, and pitch motions are neglected; in other words, $\omega = p = q = \dot{\omega} = \dot{p} = \dot{q} = 0$. In the XZ plane $y_G = 0$ is due to the symmetry of the underwater vehicle. If we apply these simplifications to the equations of motion described above, the equations become simplified for surge, sway, and yaw as shown in the Eq. (7), Eq. (8) and Eq. (9) respectively. The model developed by Abkowitz [25], solves the equations of motion for the hydrodynamic forces (X, Y) and moment (N) acting on the hull by considering the vessel as a whole and expanding them to the third-order Taylor series.

$$m(\dot{u} - vr - x_G r^2) = X \quad (7)$$

$$m(\dot{v} + ur) + mx_G\dot{r} = Y \quad (8)$$

$$I_z\dot{r} + mx_G(\dot{v} + ur) = N \quad (9)$$

The obtained forces and moments from numerical simulations of static drift maneuver are converted to non-dimensional values according to the proposal of *SNAME* [26]. These value of forces in the X, Y, and moment around Z axis are obtained by using the following formulas.

$$X' = \frac{X,Y,Z}{\frac{1}{2}\rho V^2 L^2} \quad , \quad Y' = \frac{Y}{\frac{1}{2}\rho V^2 L^2} \quad , \quad N' = \frac{N}{\frac{1}{2}\rho V^2 L^3} \tag{10}$$

2.2 Computational Model

In this study, we utilized the ANSYS Fluent software for performing CFD simulations on the DARPA Suboff model. The research focused on the fully appended (AFF-8) configuration, specifically analyzing the hydrodynamic behavior during static drift at a speed of 3.346 m/s. The main objective was to assess the longitudinal (X-force), lateral (Y-force), and yaw moment (Z-moment) under varying drift angles from 0 to 18 degrees. The second-order upwind scheme is used to discretize the governing equations employing the finite volume method. The SIMPLEC (semi-implicit method for the pressure-linked equations) algorithm is used to handle pressure-velocity coupling. SIMPLEC was chosen for its quick convergence rate since it requires less iterations and processing time, which is particularly useful for steady-state analysis [27]. The flow around the UV geometry is modeled using the incompressible steady RANS equation system.

The RANS equation which governs the principle of mass described in Eq. (11)

$$\frac{\partial y}{\partial x_i}(\rho u_i) = 0 \tag{11}$$

Where ρ is fluid density and u_i is the velocity component in each of the directions (x, y, z). Equation for conservation of momentum in each direction can be written as:

$$\frac{\partial(\rho u_i)}{\partial t} + \rho u_j \frac{\partial u_i}{\partial x_j} = \rho F_i - \frac{\partial P}{\partial x_i} + \frac{\partial}{\partial x_j}\left[\mu \frac{\partial u_i}{\partial x_j} - \rho\overline{u_i{}' u_j{}'}\right] \tag{12}$$

Where F_i is the body force, u_i is time averaged velocity components in cartesian coordinates x_i $(i = 1,2,3)$, P is the time averaged pressure, μ is the dynamic viscosity, and $\rho\overline{u_i{}' u_j{}'}$ is the Reynolds stress tensor. The time averaged Navier-Stokes equations are closed by estimating the stress tensor with several turbulence models. In the present study, *k*-ω SST turbulence model [28] is used. One of the primary advantages is its ability to accurately predict flow separation and transition from laminar to turbulent flow, which is crucial for analyzing resistance and maneuvering characteristics. The model combines the strengths of the k-ω model in the near-wall region with the k-ε model in the free stream, enhancing its versatility and robustness across a range of flow conditions. Additionally, the k-ω SST model provides improved performance for complex flows due to adverse pressure gradients and vortex shedding. The transport equation for turbulence kinetic energy k is given in Eq. (13):

$$\frac{\partial}{\partial t}(\rho k) + \frac{\partial}{\partial x_i}(\rho k u_i) = \partial x_j \partial(\Gamma_k \frac{\partial k}{\partial x_j}) + G_k - Y_k \tag{13}$$

Similarly, equation for the specific dissipation rate ω is given by Eq. (14):

$$\frac{\partial}{\partial t}(\rho\omega) + \frac{\partial}{\partial xi}(\rho\omega u_i) = \frac{\partial}{\partial x_j}(\Gamma_\omega \frac{\partial \omega}{\partial x_j}) + G_\omega - Y_\omega + D_\omega \tag{14}$$

Where ρ is the fluid density, k is the turbulence kinetic energy, Γ_k and Γ_ω is the effective diffusivity of k and ω, G_k and G_ω is the production of turbulence kinetic energy due to mean velocity gradients, Y_k and Y_ω are the dissipation of k and ω, and D_ω represents the cross-diffusion term that arises in the SST model, which accounts for the combination between the k-ω model near the wall and the k-ε model away from the wall. It ensures that the SST model retains the advantages of both models. The density of the fluid domain, i.e. freshwater is 998.2 kg/m^3 and kinematic viscosity is 0.001003 Pa-s.

2.3 Geometry of the Model

The DARPA Suboff model, known for its streamlined hull form, was selected for this study due to its extensive validation in the literature. The model's geometry, including appendages, was defined precisely to ensure accurate representation. Main parameters of the geometry are given in Table 1 and model representation is illustrated in Figure 2. The computational domain was structured to mimic real-world sea conditions, extending 2L in front, 5L at the Aft, and 2L at the sides, top, and bottom. Boundary conditions were carefully set to minimize computational artifacts and ensure the accuracy of the simulations. Front and Port side are selected as Velocity inlet, Aft and Starboard side are selected as Pressure outlet, Top and bottom are selected as symmetry, and Suboff model is selected as no slip wall. Description of the boundary conditions is given in Figure 3.

Table 1
Main parameters of DARPA Suboff Geometry (AFF-8)

Parameters	Value
Overall length (m)	4.356
Maximum diameter (m)	0.508
Centre of buoyancy l_{cb} (m)	0.4621 L_{OA}
Length between perpendiculars l_{pp} (m)	4.261
Volume(m^3)	0.706
Wetted surface area (m^2)	6.3509

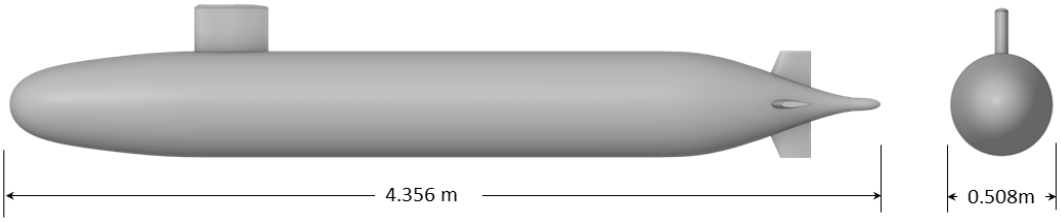

Fig. 2. 3D model of fully appended DARPA Suboff Geometry (AFF-8)

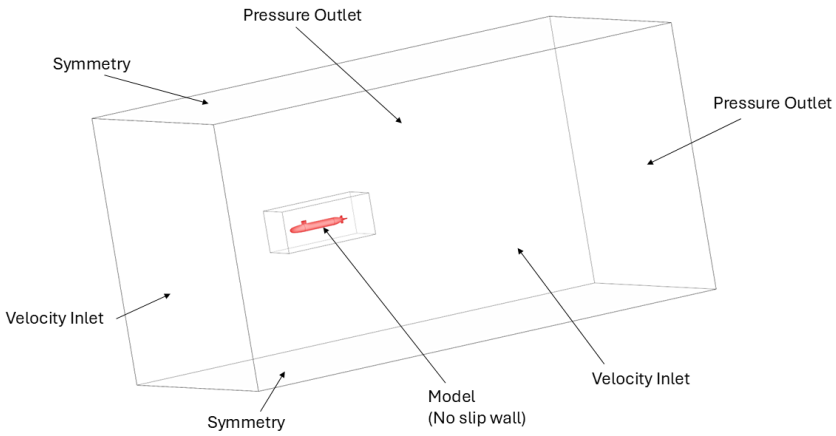

Fig. 3. Description of Boundary conditions

2.4 Meshing

Meshing the model and its corresponding domain is performed within the meshing module of ANSYS Workbench, as shown in Figure 4(a), (b), and (c). Face-meshing is implemented to discretize the model, dividing it into smaller elements for computational purposes. An enclosure was created around the model, with a deliberate strategy of gradually increasing cell size. This approach accurately captures the fluid flow behavior near the model, where finer mesh resolution is crucial for detailing intricate flow phenomena. To enhance the accuracy near the model surface, 10 inflation layers are added with first layer height of 0.51mm selected to maintain wall Y+ value within ITTC recommended range of 30<Y+<100. Conversely, the outer domain is meshed with coarser elements to maintain a manageable number of elements within the computational domain, optimizing computational efficiency and resource utilization. A grid independence study determined the optimal mesh density by testing three mesh configurations: coarse, medium, and fine.

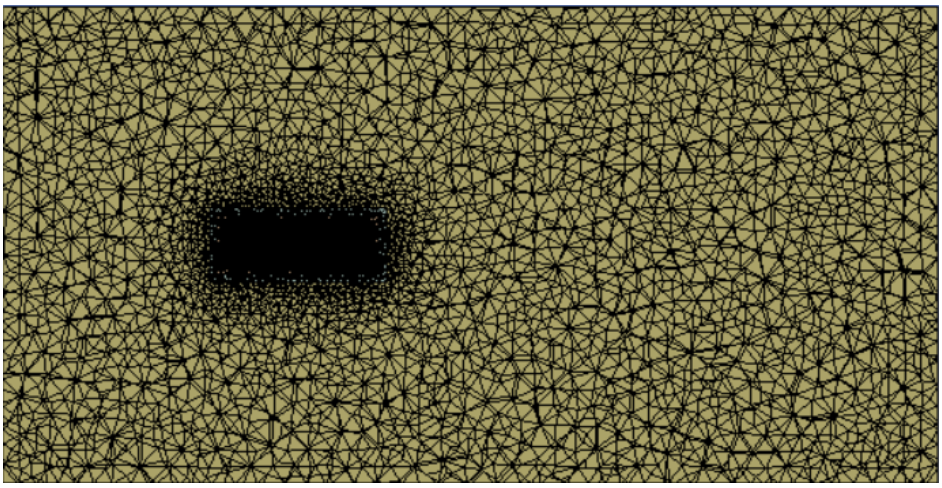

(a)

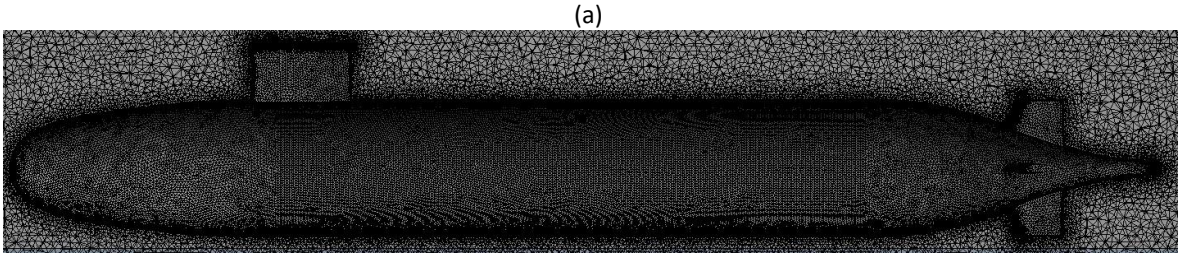

(b)

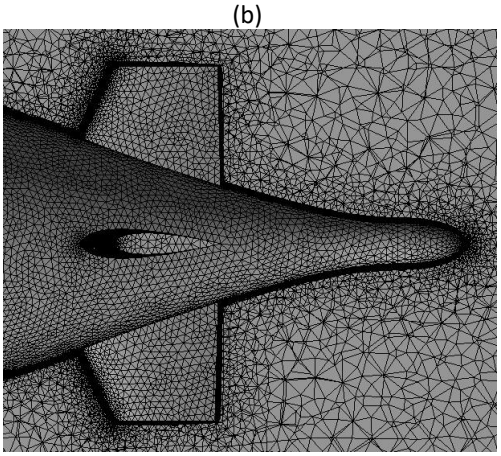

(c)

Fig. 4. (a) Meshing of Domain (b) Mesh refinement near the body (c) Local refinement for the stern appendages

2.5 Mesh Independence Study

The most reliable and straightforward approach to find the order of discretization errors in numerical simulations is by using mesh independence. In essence, for numerical results to be considered accurate and reliable, their solution must be mesh independent. A mesh independence study involves running simulations on a CFD model using progressively finer grids, reducing the mesh size in each step, until the results no longer depend on the mesh size. ITTC recommends keeping the value of refinement within the range of √2 and 2 to prevent extrapolation errors. Three different mesh sizes with a constant mesh refinement factor ($r = h_2/h_1 = h_3/h_2 = \sqrt{2}$) are chosen, where h_i is a characteristic dimension of the element. The analysis for Mesh independence study of the Suboff Geometry was conducted with zero drift angle at a velocity of 3.3436 m/s. The resulting forces and moments for each mesh were computed. Table 2 provides a description of the number of elements in each mesh and the details of longitudinal or surge force.

Table 2
Surge Force for Different Grid

Number of elements	Type	F_x
1,947,829	Coarse	-125.78 N
3,977,692	Medium	-120.675 N
7,979,491	Fine	-120.181 N

The convergence ratio, R is as follows:

$$\mathrm{R} = \frac{\epsilon_{21}}{\epsilon_{32}} \tag{15}$$

The difference between medium and fine grid solutions is $\epsilon_{21}=s_2-s_1$ and the difference between coarse and medium grids is $\epsilon_{32}=s_3-s_2$.

The situations for possible convergence are:

i. R>1 ⇒ Mesh divergence
ii. R<0 ⇒ Oscillatory convergence
iii. 0 < R <1 ⇒ Monotonic Mesh convergence

When mesh convergence happens, the convergence rate is estimated using Richardson extrapolation. Eq. (16) define the fractional difference between solutions.

$$\mathrm{e}_{ij} = \frac{(\mathrm{s}_j - \mathrm{s}_i)}{\mathrm{s}_i} \tag{16}$$

Hence, the order of the discretization is estimated in Eq. (17):

$$p = \log \frac{(e_{32}/e_{21})}{\log(r)} \tag{17}$$

Then, the mesh convergence index (GCI) is defined as:

$$GCI_{ij} = F_s \frac{|e_{ij}|}{r^p - 1} \quad (18)$$

Eq. (18) includes a safety factor, F_s, which was suggested by Roache [29] for convergence studies with a value of 1.25 for a minimum of three grids. GCI (Grid convergence index) measures the difference between the calculated and exact value. It also quantifies how the solution varies with further mesh refinement. A lower GCI value suggests that the solution is close to the exact range. Table 3 details the computed convergence ratio (R), discretization order (p), and GCI. Although, the theoretical value of p is 2, however the deviations may occur due to factors like the orthogonal grid, problem nonlinearities, and turbulence modelling, etc.

Table 3
Computed convergence ratio, the discretization order, and GCI

Parameter	Value
R	0.097
p	3.314
GCI	0.152%

The Wall Y+ value is 75, as shown in Figure 5, which is significantly good and within ITTC recommended limits.

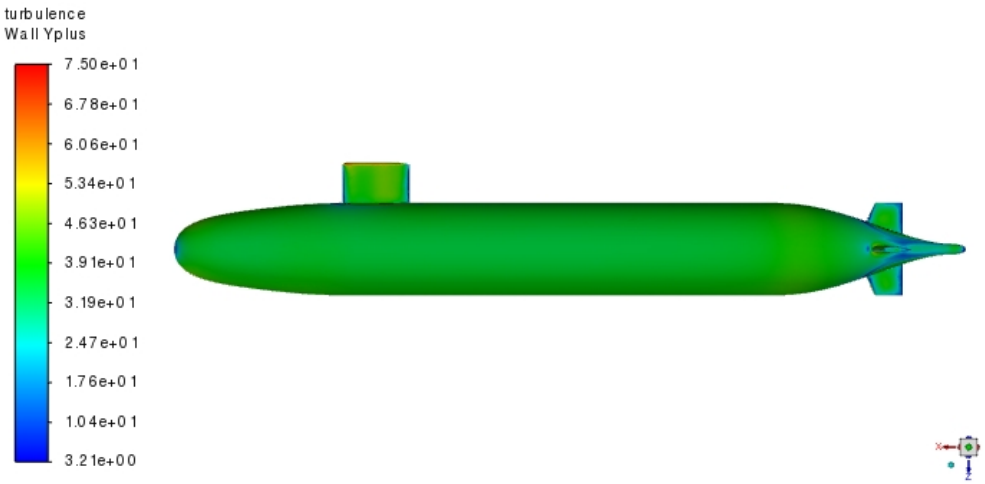

Fig. 5. Wall Y plus for medium mesh

3. Results

3.1 Hydrodynamic Forces and Moments

The simulations were performed at drift angles ranging from 0 to 18 degrees, with increments of 2 degrees. The hydrodynamic forces (X and Y) and the yaw moment (Z) were extracted and analyzed for each angle. The results are summarized in Table 4.

The longitudinal force decreases as the drift angle increases from 0 to 18 degrees. This reduction is due to changes in flow separation around the vehicle, which lowers the pressure drag. The lateral force increases significantly with the drift angle. This indicates a strong lateral force acting on the vehicle, affecting its maneuverability and stability. Similarly, the yaw moment also increases with the drift angle, reaching its maximum at 18 degrees. It is due to increased rotational forces, impacting yaw stability. This underscores the need for effective control surfaces to manage rotational forces during maneuvering.

Table 4
Forces and moment for different drift angles

Drift Angle	X-forces (N)	Y-forces (N)	Z-moment (Nm)
0	-120.6754	0.6202	0.5801
2	-118.266	92.2219	209.5935
4	-115.4781	194.925	435.704
6	-110.7965	307.9590	625.4376
8	-101.3682	451.5819	749.7396
10	-91.5989	604.9124	938.2332
12	-80.7531	752.5819	1075.347
14	-108.552	769.0785	1038.653
16	-96.9114	951.4819	1116.855
18	-82.8189	1143.9199	1194.1359

3.2 Non-Dimensional Description of Forces and Moments

The process of non-dimensionalizing the maneuvering forces and moments is performed in accordance with Eq. (10). The obtained results from CFD simulations are compared with the experimental results of the AFF-8 geometry from DTRC [11]. Experimental data and computational fluid dynamics (CFD) results are compared to confirm the accuracy of the numerical model. It also highlights strengths and areas of improvement in numerical model. The non-dimensional hydrodynamic coefficients showed good agreement with the experimental results, with deviations within acceptable ranges, particularly at lower angles of drift.

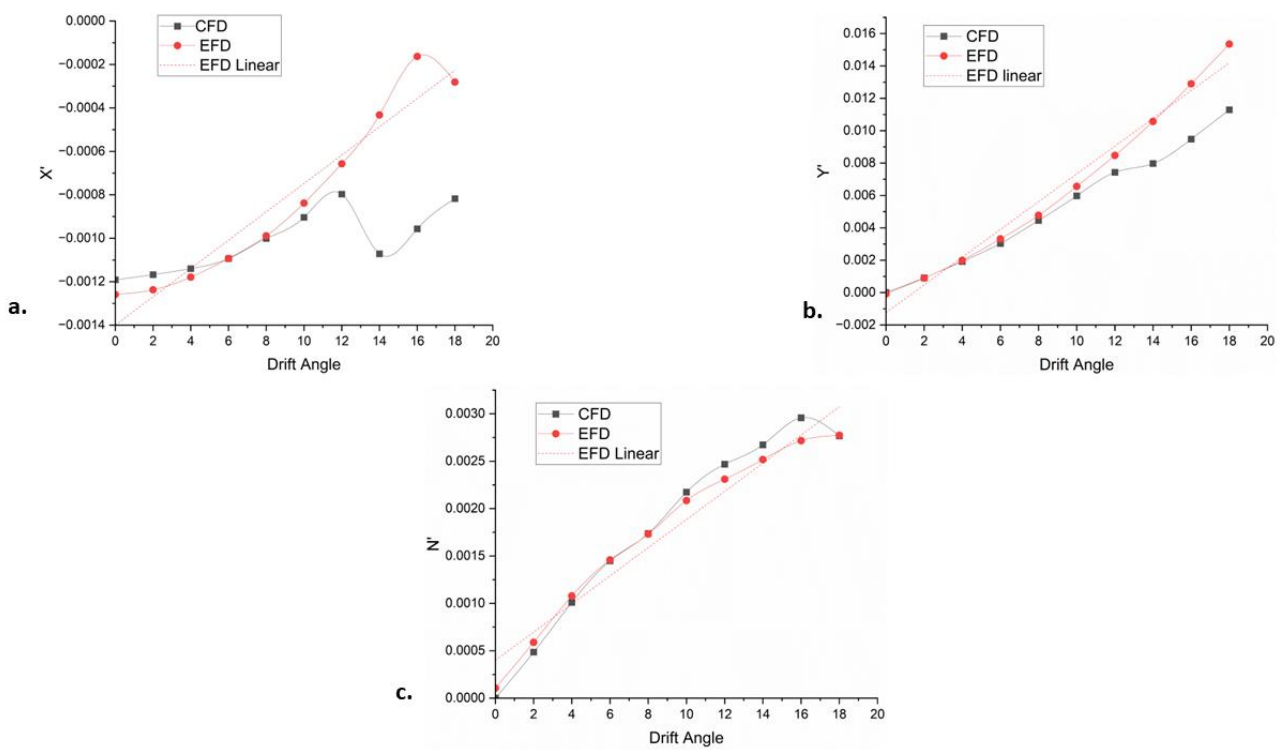

Fig. 6. Comparison between CFD results (black) and experiment data (red) of X' (a), Y'(b) and N'(c), Linear Line is plotted for EFD in dashed(red)

The validation confirmed the reliability of the RANS-based simulations using the k-ω SST turbulence model in capturing the complex flow dynamics around the Suboff model. The results

demonstrate the significant influence of drift angle on the hydrodynamic performance of the Suboff model. The decreasing trend in longitudinal force with increasing drift angle suggests potential energy savings during maneuvers involving large drift angles as the vehicle might experience reduced resistance in these conditions. However, the substantial increase in lateral forces and yaw moments indicates challenges in maintaining stability and control. The rise in lateral forces and moments can lead to difficulties in maneuverability, requiring more sophisticated control strategies to ensure the course stability of the vehicle.

3.3 Hydrodynamic Coefficients

Hydrodynamic coefficients can be obtained from numerical simulations of underwater vehicles in static drift conditions. Eq. (19), Eq. (20) and Eq. (21) can be used to predict hydrodynamic coefficients that are based on the longitudinal forces and lateral forces, and yaw moments [30].

$$X = X_v + X_{vv}v^2 \tag{19}$$
$$Y = Y_v v + Y_{vvv}v^3 \tag{20}$$
$$N = N_v v + N_{vvv}v^3 \tag{21}$$

Subsequently, in non-dimensional representation of the drift angle, these forces and moments are calculated against the sway velocity ($v = -U\,sin\beta$). The non-dimensional representation for the force and moments is obtained by using Eq. (10), and the non-dimensional vehicle's speed is $U = \sqrt{(u^2 + v^2)}$. Table 5 shows the obtained results from CFD simulation and compared with experimental results from DTRC.

Table 5
Non-Dimensional Hydrodynamic Coefficients of DARPA Suboff Geometry

Hydrodynamic Coefficient	CFD (Present)	EFD (DTRC)	Difference (%)
X'_{vv}	-0.0023	-	-
Y'_{v}	-0.0271	-0.0278	2.6
Y'_{vvv}	-0.0521	-	-
N'_{v}	-0.0132	-0.0136	3.03
N'_{vvv}	-0.066	-	-

The hydrodynamic coefficients obtained from the CFD results demonstrate a strong correlation with the experimental data, which enhances the reliability of the numerical method. This finding suggests that CFD can serve as a cost-effective substitute for lengthy physical testing. Future work will focus on expanding the study to encompass more complex circumstances, such as unsteady maneuvers, and investigating the impact of various flow regimes on hydrodynamic performance. Furthermore, an investigation of the influence of control surfaces and appendages on the underwater vehicle's overall stability and maneuverability will be conducted.

4. Conclusions

This study used ANSYS Fluent CFD simulations to evaluate the DARPA Suboff model's hydrodynamic performance at different drift angles, focusing on longitudinal and lateral forces, and yaw moments. The results clearly showed that as the drift angle increased from 0 to 18 degrees, the longitudinal force decreased while the lateral force and yaw moments increased substantially,

emphasizing the impact on the underwater vehicle's maneuverability. Converting the results to non-dimensional forces, provided a clearer understanding of the hydrodynamic performance and facilitated comparison with experimental data of DTRC. The study also estimated key maneuvering coefficients crucial for predicting underwater vehicle behavior. The findings align with the research objectives, demonstrating the effectiveness of CFD simulations in predicting the hydrodynamic behavior of underwater vehicles. However, further studies are recommended to enhance the accuracy of these simulations, including more detailed experimental validation and the exploration of different turbulence models and computational techniques. This research contributes to the broader understanding of underwater vehicle hydrodynamics and provides a foundation for future investigations aimed at optimizing underwater vehicle performance. These insights also emphasize the necessity for ongoing research to refine these techniques for better precision and applicability in real-world scenarios.

Acknowledgement
This research was not funded by any grant.

References

[1] Mucha, Philipp. "Interconnected Fluid and System Dynamics Simulations of Submarine Maneuvering for Concept Design." In *SNAME Maritime Convention*, p. D011S001R003. SNAME, 2023. https://doi.org/10.5957/SMC-2023-009
[2] AMitra, A., J. P. Panda, and H. V. Warrior. "The hydrodynamic characteristics of Autonomous Underwater Vehicles in rotating flow fields." *Proceedings of the Institution of Mechanical Engineers, Part M: Journal of Engineering for the Maritime Environment* 238, no. 3 (2024): 691-703. https://doi.org/10.1177/14750902231181843
[3] Anuar, Kaspul, and Agung Soegihin. "Aerodynamic Analysis of Unnamed Aerial Vehicle Serindit V-2 Using Computational Fluid Dynamics." *Journal of Advanced Research in Fluid Mechanics and Thermal Sciences* 93, no. 1 (2022): 83-93. https://doi.org/10.37934/arfmts.93.1.8393
[4] Hoa, Nguyen Thi Ngoc, and Tat-Hien Le. "Numerical Simulation Flow Around the Containership by using CFD Method." *Journal of Advanced Research in Fluid Mechanics and Thermal Sciences* 117, no. 1 (2024): 203-213. https://doi.org/10.37934/arfmts.117.1.203213
[5] Le Tat, Hien, and Tran Van Tao. "Numerical Investigation of the Scale Effect on the Flow around the Ship by using RANSE Method." *CFD Letters* 15, no. 11 (2023): 67-78. https://doi.org/10.37934/cfdl.15.11.6778
[6] Ahmed, Alaaeldeen Mohamed Elhadad. "Comparative investigation of resistance prediction for surface combatant ship model using CFD modeling." *Journal of Advanced Research in Fluid Mechanics and Thermal Sciences* 107, no. 2 (2023): 225-235. https://doi.org/10.37934/arfmts.107.2.225235
[7] Zhang, Dapeng, Bowen Zhao, Yi Zhang, and Nan Zhou. "Numerical simulation of hydrodynamics of ocean-observation-used remotely operated vehicle." *Frontiers in Marine Science* 11 (2024): 1357144. https://doi.org/10.3389/fmars.2024.1357144
[8] Aryawan, Wasis Dwi, I. Ketut Aria Pria Utama, and Yuda Apri Hermawan. "CFD Analysis into the Resistance Characteristics of Remotely Operated Vehicles when Submerges Under Water and Sails on the Surface." *CFD Letters* 15, no. 8 (2023): 166-178. https://doi.org/10.37934/cfdl.15.8.166178
[9] Begovic, Ermina, Saeid Panahi, Barbara Rinauro, and Gennaro Rosano. "Determination of Hydrodynamic Maneuvering Coefficients of a Planing Hull Using CFD with the Aid of SDT." In *HSMV 2023*, pp. 65-77. IOS Press, 2023. https://doi.org/10.3233/PMST230010
[10] Groves, Nancy C., Thomas T. Huang, and Ming S. Chang. *Geometric characteristics of DARPA SUBOFF models (DTRC Model Nos. 5470 and 5471)*. David Taylor Research Center, 1989.
[11] R. Roddy, "Investigation of the Stability and Control Characteristics of Several Configurations of the DARPA Suboff Model (DTRC Model 5470) from Captive-Model Experiments," Sep. 1990.
[12] Huang, T., and H. L. Liu. "Measurements of flows over an axisymmetric body with various appendages in a wind tunnel: the DARPA SUBOFF experimental program." (1994).
[13] "ITTC Manoeuvring Committee. (2014). Final report and recommendations to the 27th ITTC. Proceedings of the 27th International Towing Tank Conference, Copenhagen, Denmark."
[14] Toxopeus, Serge, and Guilherme Vaz. "Calculation of current or manoeuvring forces using a viscous-flow solver." In *International Conference on Offshore Mechanics and Arctic Engineering*, vol. 43451, pp. 717-728. 2009. https://doi.org/10.1115/OMAE2009-79782

[15] Vaz, Guilherme, Serge Toxopeus, and Samuel Holmes. "Calculation of manoeuvring forces on submarines using two viscous-flow solvers." In *International Conference on Offshore Mechanics and Arctic Engineering*, vol. 49149, pp. 621-633. 2010. https://doi.org/10.1115/OMAE2010-20373

[16] Pan, Yu-cun, Huai-xin Zhang, and Qi-dou Zhou. "Numerical prediction of submarine hydrodynamic coefficients using CFD simulation." *Journal of Hydrodynamics* 24, no. 6 (2012): 840-847. https://doi.org/10.1016/S1001-6058(11)60311-9

[17] Atik, Hediye. "Türbülans modellerinin DARPA SUBOFF statik sürükleme testi üzerinden incelenmesi." *Gazi Üniversitesi Mühendislik Mimarlık Fakültesi Dergisi* 37, no. 3 (2021): 1509-1522. https://doi.org/10.17341/gazimmfd.748378

[18] Le Tat, Hien, Nguyen Duy Anh, and Nguyen Thi Ngoc Hoa. "Numerical Investigate the Effect of Turbulence Models on the CFD Computation of Submarine Resistance." *CFD Letters* 16, no. 10 (2024): 126-139. https://doi.org/10.37934/cfdl.16.10.126139

[19] Firdhaus, Ahmad, Muhammad Luqman Hakim, Good Rindo, and Muhammad Iqbal. "Ship performances CFD analysis of hydrofoil-supported high-speed catamaran hull form." *Journal of Advanced Research in Fluid Mechanics and Thermal Sciences* 113, no. 1 (2024): 108-121. https://doi.org/10.37934/arfmts.113.1.108121

[20] Bao, Han, Haitao Zhu, and Di Liu. "Research on Hydrodynamic Modeling and Simulation of Streamlined Autonomous Underwater Vehicle based on CFD Method." In *2023 35th Chinese Control and Decision Conference (CCDC)*, pp. 4795-4800. IEEE, 2023. https://doi.org/10.1109/CCDC58219.2023.10327061

[21] Elhadad, Alaaeldeen M., and Abo El-Ela. "Experimental and Cfd Resistance Validation of Naval Combatant Dtmb 5415 Model." *Experimental and Cfd Resistance Validation of Naval Combatant Dtmb* 5415 (2023). https://doi.org/10.2139/ssrn.4418749

[22] Jones, David A., David B. Clarke, Ian B. Brayshaw, Jean L. Barillon, and Brendon Anderson. *The calculation of hydrodynamic coefficients for underwater vehicles*. 2002.

[23] Thor I. Fossen, "Guidance and Control of Ocean Vehicles," *Chichester: Wiley*, 1994.

[24] Kim, Dong-Hwi, Yagin Kim, Hyung-Min Baek, Young-Myung Choi, Young Jun Kim, Hongrae Park, Hyeon Kyu Yoon *et al.,* "Experimental study of the hydrodynamic maneuvering coefficients for a BB2 generic submarine using the planar motion mechanism." *Ocean Engineering* 271 (2023): 113428. https://doi.org/10.1016/j.oceaneng.2022.113428

[25] MA, ABKOWITZ. "Lectures on ship hydrodynamics-steering and maneuvering." *Hydro-and aerodynamics laboratory report Hy-5* (1964).

[26] *Nomenclature for Treating the Motion of a Submerged Body Through a Fluid: Report of the American Towing Tank Conference*. Society of Naval Architects and Marine Engineers, 1950.

[27] Oliveira, Jean Michael Borges de, Luciano Kiyoshi Araki, Marcio Augusto Villela Pinto, and Simone de Fátima Tomazzoni Gonçalves. "An alternative full multigrid SIMPLEC approach for the incompressible Navier–Stokes equations." *Numerical Heat Transfer, Part B: Fundamentals* 83, no. 6 (2023): 410-432. https://doi.org/10.1080/10407790.2023.2167752

[28] Menter, Florian R. "Two-equation eddy-viscosity turbulence models for engineering applications." *AIAA journal* 32, no. 8 (1994): 1598-1605. https://doi.org/10.2514/3.12149

[29] Roache, Patrick J. "Quantification of uncertainty in computational fluid dynamics." *Annual review of fluid Mechanics* 29, no. 1 (1997): 123-160. https://doi.org/10.1146/annurev.fluid.29.1.123

[30] Muhammad, A. H., D. Paroka, S. Rahman, M. I. Nikmatullah, and L. Sudirman. "Hydrodynamic Derivatives of a Ferry Ship Maneuvering in Deep and Shallow Water with Computational Fluid Dynamic Method." In *IOP Conference Series: Earth and Environmental Science*, vol. 1198, no. 1, p. 012008. IOP Publishing, 2023. https://doi.org/10.1088/1755-1315/1198/1/012008